International Journal of Computational Fluid Dynamics, 2002 Vol. 16 (1), pp. 65–82

Numerical Study of the Flow Behind a Rotary Oscillating Circular Cylinder

XI-YUN LU*

Department of Modern Mechanics, University of Science and Technology of China, Hefei, Anhui 230026, People's Republic of China

(Received 30 October 2000; In final form 18 April 2001)

A numerical study is performed of flow behind a rotationally oscillating circular cylinder in a uniform flow by solving the two-dimensional incompressible Navier–Stokes equations. The flow behavior in lock-on regime and the timing of vortex formation from the oscillating cylinder are studied. When the frequency of excitation of the cylinder is in the vicinity of the natural vortex formation frequency, a lock-on vortex formation regime appears. As the excitation frequency being increased relative to the natural frequency the initially formed vorticity concentration switches to the opposite side of the cylinder. The effects of oscillating frequency and amplitude on the vortex structures formed in the near wake of the cylinder are also investigated. Based on the present calculated results, some complicated vortex patterns are identified and are consistent with the previous experimental visualizations.

Keywords: Vortex formation; Vortex control; Separation flow; Lock-on; Circular cylinder; Oscillatory flow; Finite difference method

1. INTRODUCTION

Viscous flow past a bluff body has received a great deal of attention owing mainly to its theoretical and practical significance. The presence of vortex shedding, together with vortex wakes, is related to pressure fluctuation, structural vibration, and noise. It is necessary to find ways to control the unsteady separated flows in the wake. There have been many approaches to control the formation and shedding of vortices from a circular cylinder. In general, simple geometrical configurations have been employed, e.g. splitter plate by Unal and Rockwell (1987); Kwon and Choi (1996), second cylinder by Strykowski and Sreenivasan (1990). And direct disturbed methods were also used, such as, oscillatory inlet flow by Barbi et al. (1986) and Sarpkaya (1986), localized surface excitation with suction and blowing by Williamson and Roshko (1988), and vibrating cylinder by Nakano and Rockwell (1993), Lu and Dalton (1996) and Lu et al. (1997). Some researchers, e.g. Roussopoulos (1993) and Park et al. (1994), have also put their interests on the feedback control of vortex shedding at low Reynolds numbers ($Re < 100$). A rotary oscillation has also been contemplated by Taneda (1978), Filler et al. (1991) and Tokumaru et al. (1991,1993). Because of the rotary oscillation of a cylinder, overall characteristics of the vortex shedding and wake patterns were altered significantly. Therefore, an investigation of this problem still has its significance of the vortex control and the feedback control of vortex shedding because the rotation rates are easily manipulated by a simple approach.

Three parameters governing the development of a rotationally oscillating circular cylinder in a uniform flow are the Reynolds number, defined as $Re = 2UR/\nu$, where U is the uniform approach velocity, ν is the kinematic viscosity and R is the radius of the circular cylinder; the maximum angular displacement θ_{max}; and the oscillating frequency f_e. Experimental studies of an approach flow past a rotationally oscillating circular cylinder were conducted. Taneda (1978) examined the effects of rotational oscillation at $Re = 30-300$, and indicated that, at very high oscillating frequencies and magnitudes, the vortex shedding process could be nearly eliminated. Filler et al. (1991) have experimentally studied the frequency response of the shear layers separating from a circular cylinder subjected to small-amplitude rotational oscillations for $Re = 250-1200$. Tokumaru et al. (1991,1993) have shown that rotational oscillation at very large magnitudes can produce significant reductions in drag on the cylinder. They have also investigated the

*Fax: +86-551-3631760. E-mail: xlu@ustc.edu.cn

ISSN 1061-8562 © 2002 Taylor & Francis Ltd
DOI: 10.1080/10618560290004035

mean lift variation of a circular cylinder executing both steady rotation and rotary oscillation with a net rotation rate in a uniform flow.

A comparatively smaller number of researchers have numerically investigated the effects of rotational oscillation of the cylinder. Lu and Sato (1996) investigated numerically the vortex formations behind a rotary oscillating circular cylinder. Lu (1996) also studied the development of the wake behind a circular cylinder impulsively started into rotatory and rectilinear motion. Baek and Sung (1998) have performed a numerical simulation of the flow behind a rotary oscillating circular cylinder at $Re = 110$. Recently, Buldakov et al. (2000) studied a steady two-dimensional incompressible flow past a rapidly rotating cylinder with suction, based on high-Reynolds-number asymptotic analysis of incompressible Navier–Stokes equations. Dennis et al. (2000) used a series expansion for small time to investigate the temporal development of two-dimensional viscous incompressible flow induced by an impulsively started circular cylinder which performs time-dependent rotational oscillations about its axis and translates at right angles to the axis. Then Baek and Sung (2000) took a numerical analysis for the quasi-periodicity in the wake where a circular cylinder is rotationally oscillated in time at $Re = 110$. Their main emphasis is placed on the identification of frequency selection subjected to the controlled perturbations in the vicinity of lock-on. Additionally, a number of researchers, e.g. Badr and Dennis (1985) and Chen et al. (1993), have computationally studied a single directional rotary circular cylinder moving in a uniform flow. A fairly full account of an unsteady flow past a rotating cylinder is given by Badr et al. (1990).

To get general conclusions of viscous flow past a rotary oscillating circular cylinder, some calculations in the present study have been performed over the range of the parameters of $Re = 300-1000$, $f_e/f_o = 0.5-4.0$, and $\theta_{max} = 15-90^\circ$, where f_o represents natural vortex shedding frequency. Vortex forming and shedding behind a rotationally oscillating circular cylinder in a uniform flow is investigated. The primitive-variable form of the Navier–Stokes equations for incompressible flows is numerically solved by a fractional-step method developed by Kim and Moin (1985). The flow behavior in the vicinity of lock-on regime and the timing of vortex formation from the oscillating cylinder are studied. Further the effects of oscillating frequency and amplitude on the vortex structures formed in the near wake of the cylinder are investigated, and some vortex patterns, based on the present calculated results, are also identified.

2. GOVERNING EQUATIONS

A non-rotating reference frame fixed to the axis of the circular cylinder is used. In this frame, the fluid at infinity has a uniform stream with the velocity U in the x-direction, and the cylinder has an oscillatory rotation. It is supposed that the uniform translation and oscillating rotation of the cylinder start impulsively at the same instant, and the flow is two-dimensional. The incompressible Navier–Stokes equations with primitive variables are used for the calculation. In dimensionless form and in polar coordinates (r,θ), these equations read

$$\frac{\partial u}{\partial r} + \frac{u}{r} + \frac{1}{r}\frac{\partial v}{\partial \theta} = 0, \tag{1}$$

$$\frac{\partial u}{\partial t} + u\frac{\partial u}{\partial r} + v\frac{\partial u}{r\partial \theta} - \frac{v^2}{r} = -\frac{\partial p}{\partial r} + \frac{2}{Re}\left(\nabla^2 u - \frac{2}{r^2}\frac{\partial v}{\partial \theta} - \frac{u}{r^2}\right), \tag{2}$$

$$\frac{\partial v}{\partial t} + u\frac{\partial v}{\partial r} + v\frac{\partial v}{r\partial \theta} + \frac{uv}{r} = -\frac{\partial p}{r\partial \theta} + \frac{2}{Re}\left(\nabla^2 v + \frac{2}{r^2}\frac{\partial u}{\partial \theta} - \frac{v}{r^2}\right), \tag{3}$$

where the cylinder radius R and the approach velocity U are used as the length and velocity scales, respectively; u, v are the dimensionless radial and circumferential velocity components, respectively, p is the dimensionless pressure, and the Laplace operator ∇^2 is

$$\nabla^2 = \frac{\partial^2}{\partial r^2} + \frac{1}{r}\frac{\partial}{\partial r} + \frac{1}{r^2}\frac{\partial^2}{\partial \theta^2}. \tag{4}$$

In the present calculation, the initial field is taken as the two-dimensional potential flow over stationary cylinder. The rotation of the cylinder enters in the boundary conditions, of which the dimensionless form is

$$u = 0, \quad v = v_B = 2\pi f_e \theta_{max} \sin(2\pi f_e t), \tag{5}$$

on the body surface ($r = 1$), and

$$u = \left(1 - \frac{1}{r^2}\right)\cos\theta, \quad v = -\left(1 + \frac{1}{r^2}\right)\sin\theta, \quad u_e < 0, \tag{6}$$

$$\frac{\partial u}{\partial r} = \frac{2}{r^3}\cos\theta, \quad \frac{\partial v}{\partial r} = \frac{2}{r^3}\sin\theta, \quad u_e \geq 0, \tag{7}$$

at outer boundary, where u_e is the radial velocity component that is normal to the outer boundary. In the circumferential direction, periodic boundary conditions are employed.

3. NUMERICAL METHOD

The Navier–Stokes equations in vector form are written as,

$$\frac{\partial V}{\partial t} = -\nabla p + L(V) + N(V), \tag{8}$$

where V is the velocity vector; L(V) and N(V) represent

viscous and convective terms, respectively:

$$L(V) = \frac{2}{Re}\nabla^2 V, \tag{9}$$

$$N(V) = -(V\cdot\nabla)V. \tag{10}$$

Using the fractional-step method proposed by Kim and Moin (1985), the semi-discrete form of Eq. (8) can be obtained by splitting Eq. (8) into two substeps as

$$\frac{\hat{V} - V^n}{\Delta t} = N_D(V) + L_D(V), \tag{11}$$

$$\frac{V^{n+1} - \hat{V}}{\Delta t} = -\nabla p^{n+1/2}, \tag{12}$$

where $\hat{V}$ is an intermediate velocity, $L_D(V)$ and $N_D(V)$, respectively, denote discretized forms of L(V) and N(V). In the splitting method, it is required that the velocity field V^{n+1} satisfy the incompressibility constraint,

$$\nabla\cdot V^{n+1} = 0. \tag{13}$$

Incorporating the incompressibility constraint into Eq. (12), we finally arrive at a separately solvable elliptic equation for the pressure in the form,

$$\nabla^2 p^{n+1/2} = \frac{1}{\Delta t}\nabla\cdot\hat{V}. \tag{14}$$

To solve the elliptic Eq. (14), a pressure boundary condition must be implemented, which is a key factor for solving the incompressible Navier–Stokes equations. According to Gresho and Sani (1987), the pressure condition on the body surface is given by

$$\frac{\partial p}{\partial r} = -\frac{2}{Re}(\nabla\times\nabla\times V)\cdot n_r + \frac{v_B^2}{r}, \tag{15}$$

where n_r indicates the unit vector at the radial direction, and v_B is given in Eq. (5).

In this study, a staggered grid, which is uniformly spaced in the circumferential direction and exponentially stretched in the radial direction, is employed for the discretization of the governing equations. The transformation is given as

$$r = e^{\pi\xi}, \quad \theta = \pi\eta, \tag{16}$$

where $0 \le \xi < \xi_\infty$, $0 \le \eta \le 2$. The convective terms in Eq. (11) are approximated using a third-order biased upwind difference scheme in Kawamura and Kuwahara (1984) with all other spatial derivatives being discretized using a second-order central difference scheme. The time derivative in Eq. (11) is solved using a second-order Adams–Bashforth scheme.

The computational loop to advance the solution from one time level to the next consists of the following three substeps. First, discretized form of Eq. (11) is advanced explicitly to obtain the new intermediate velocity, using a second-order Adams–Bashforth scheme. Then, using the known intermediate velocity, the pressure Poisson Eq. (14) is solved for the new pressure field. Finally, Eq. (12) is solved for the new velocity.

4. RESULTS AND DISCUSSION

In the present calculation, the number of mesh points for the calculations was 256×128 in the r and θ directions. The computational domain is 50R in the radial direction, and time step is 0.001. It has been determined that the computed results are independent of the time steps and the grid sizes. As an example, the results calculated by two grid systems: $(r, \theta) = 256\times128$ with $\Delta t = 0.001$ and $(r, \theta) = 512\times256$ with $\Delta t = 0.0005$ were compared for approach flow past the cylinder at $Re = 300$. They produced virtually identical results as shown in Fig. 1; the only difference being a small phase lag for the fine grid. The phase lag is attributed to the onset of the wake instability leading to vortex shedding. A similar convergence check has been done for other Reynolds numbers (not shown here). From Fig. 1, the Strouhal number defined usually by using the length scale of the cylinder diameter, as determined from the lift coefficient plot, is 0.206 (or $f_o = 0.103$ based on the length scale of

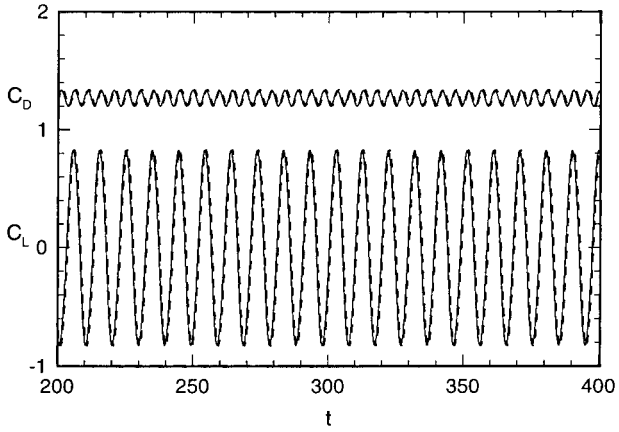

FIGURE 1 Lift and drag coefficients for different grid resolutions and time steps for flow past a stationary cylinder at $Re = 300$: solid lines, 256×128, $\Delta t = 0.001$; dashed lines, 512×256, $\Delta t = 0.0005$.

the cylinder radius), which compares quite well with the experimental value of approximately 0.21.

In order to get general conclusions of the flow past a rotary oscillating circular cylinder, some calculations over the range of the parameters of Re = 300–1000, f_e/f_o = 0.5–4.0, and θ_{max} = 15–90° were performed. For brevity, only some typical results were mainly discussed in the following sections.

4.1. Flow Behavior Near Lock-on Regime

If the lock-on appears for the flow past an oscillating rotation cylinder, vortex shedding frequency is subjected to the imposed forcing rotational frequency (f_e). The vortex structures in the near wake repeat from cycle to cycle of the rotating oscillation. As Karniadakis and Triantafyllou (1989) used the phase diagram and power spectral density to identify the flow regimes in a numerical study of unforced and forced laminar flow over a circular cylinder, the phase diagrams (velocity end-point diagram in u–v plane) at one point in the near wake are therefore shown in Fig. 2 for some typical cases of θ_{max} = 45°, Re = 300, and f_e = 0.07, 0.08, 0.12 and 0.13. The corresponding time evolution of lift and drag coefficients is also shown in Fig. 3. The lock-on criterion can be discriminated by checking both the phase diagram and the lift and drag coefficients variation, which is known to be sensitive to the flow structure near the cylinder. As shown in Fig. 2, the velocity phase diagrams clearly show that the flow is periodic for f_e = 0.08 and 0.12, but non-periodic for f_e = 0.07 and 0.13. The vortex shedding frequency can be obtained from the evolution of the lift and drag coefficients shown in Fig. 3. Thus, it is clearly captured that the lock-on cases are at f_e = 0.08 and 0.12, and nonlock-on cases at f_e = 0.07 and 0.13.

The cylinder, in this problem, takes both motions at the same instant, i.e. oscillatory rotation and translation. If the oscillatory rotation dominates the flow, preferred vortex modes may be synchronized with the cylinder rotation, and the vortex shedding frequency mainly depends on the forcing oscillatory frequency (f_e). Otherwise, for the limiting condition of V_B = 0, this problem becomes an approach flow past a stationary cylinder. So, if the approach flow dominates the flow field, a preferred vortex

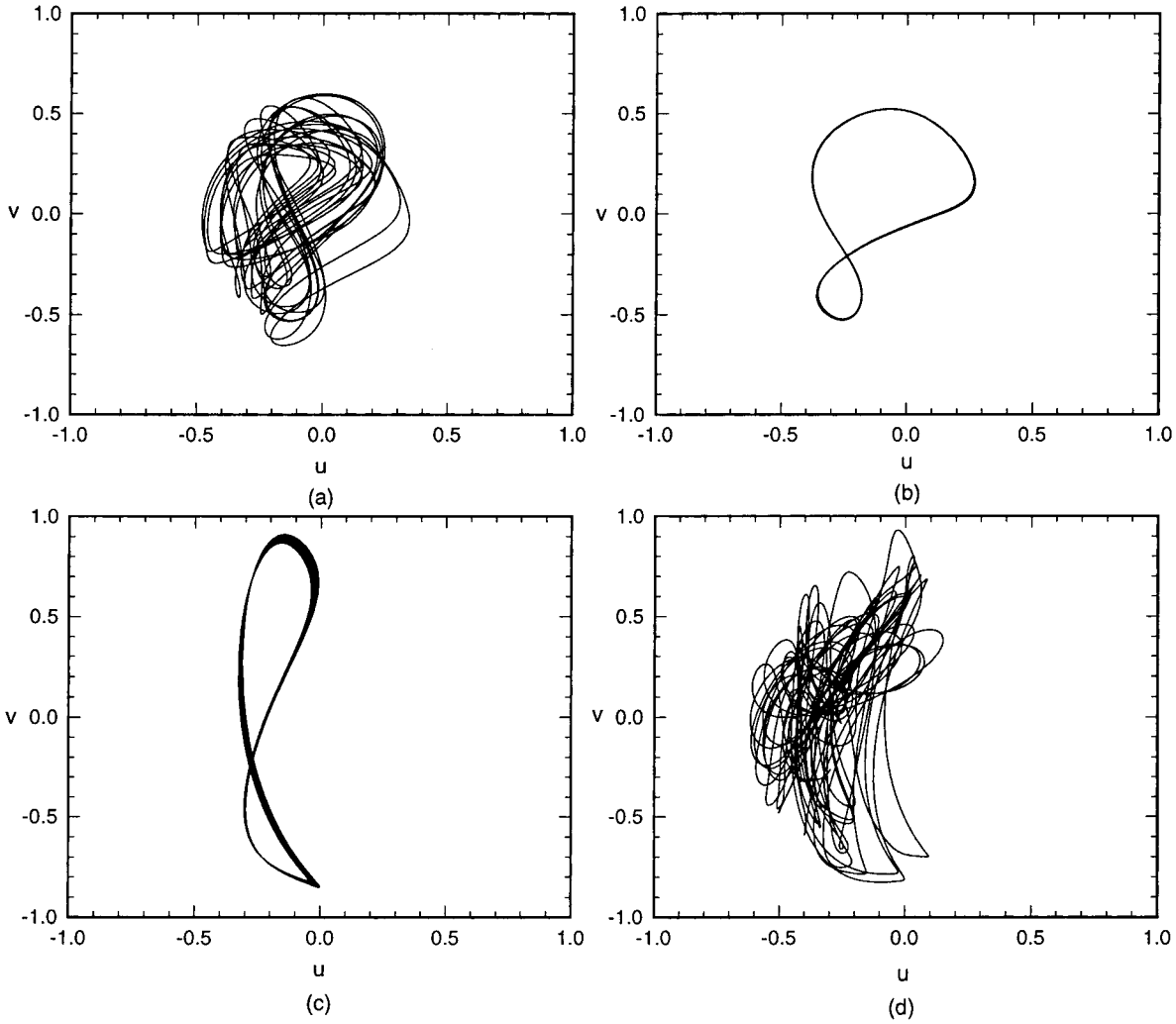

FIGURE 2 Phase diagram (velocity end-point diagram in u–v plane) from t = 200–400 at point of x = 1.8228 and y = 0.2704 for θ_{max} = 45°, Re = 300, and f_e = (a) 0.07, (b) 0.08, (c) 0.12 and (d) 0.13.

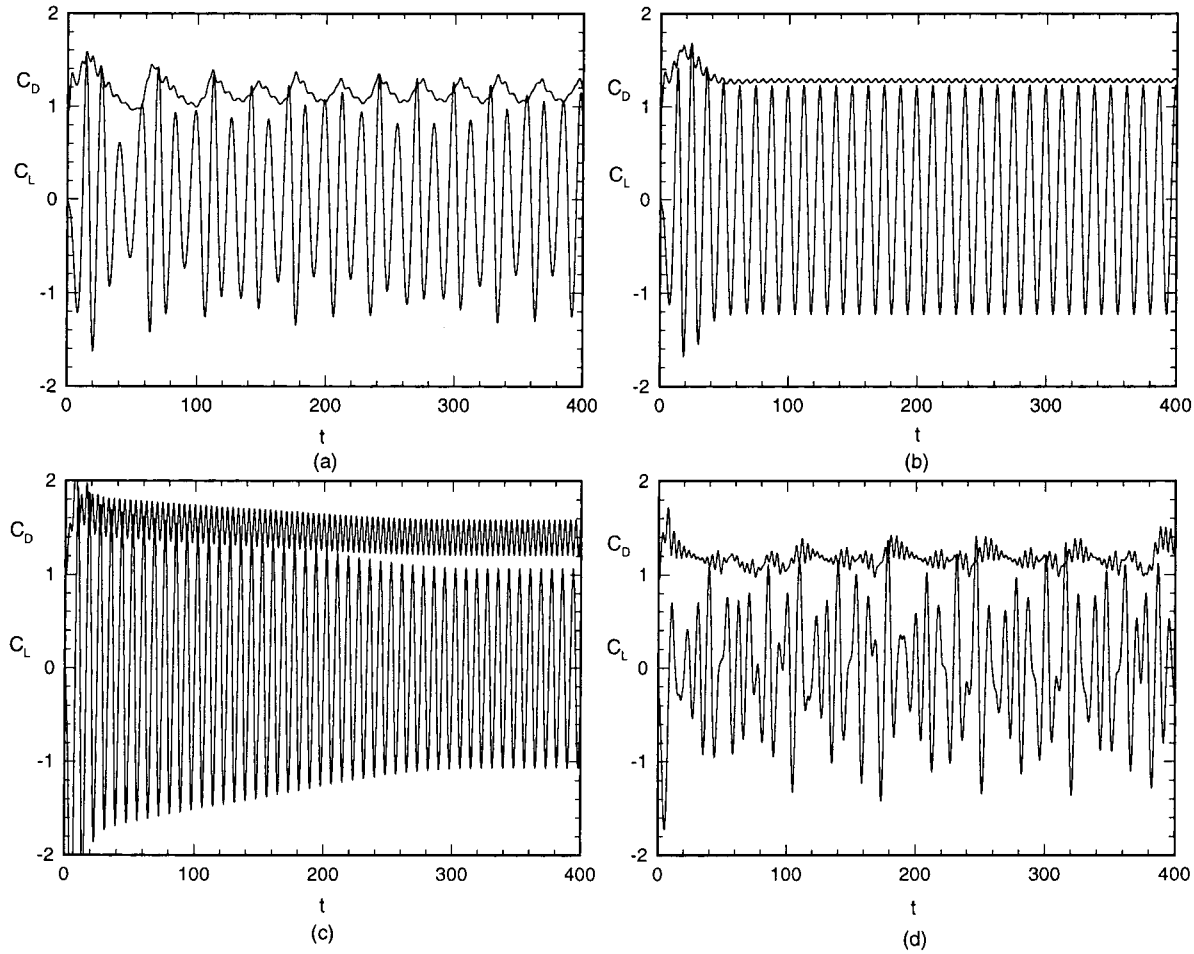

FIGURE 3 Lift and drag coefficients for $\theta_{max} = 45°$, Re = 300, and f_e = (a) 0.07, (b) 0.08, (c) 0.12 and (d) 0.13.

mode may be the formation of a wake flow similar to the Karman vortex street with a natural vortex shedding frequency f_o. In the nonlock-on region, competition and nonlinear interaction between the rotating and translating disturbances occur. Figure 4 shows the power spectrum density (PSD) of the lift coefficients which are shown in Fig. 3 for $f_e = 0.07$ and 0.08. As described above, due to the flow at $f_e = 0.08$ laying in lock-on regime, only a single basic frequency, i.e. forcing frequency f_e, and its superharmonic modes are excited, as shown in Fig. 4b. Correspondingly, when the forcing frequency is out of the lock-on regime, as shown in Fig. 4a at $f_e = 0.07$, many frequencies, which are the forcing frequency f_e the natural frequency f_o, their harmonics, and even the sum and difference of the two basic frequencies, such as $f_o - f_e$, $f_o + f_e$, etc. are excited. In general, the vortex modes competition and nonlinear interaction have global influence on the flow field to control the unsteady separated flows in the wake, which has also been observed by Wu et al. (1998) for the post-stall flow control on an airfoil by local unsteady forcing.

Figure 5 shows the distribution of the maximum values of the lift coefficient (C_L), where the flows are within the lock-on region. When the lock-on flow occurs, the rotationally oscillating frequency is synchronized and resonated with the vortex shedding frequency, and the amplitude of C_L is larger than that of the non-oscillation case. As θ_{max} increases, the forcing frequency range, in which lock-on flow appears, is widened. This trend also confirms the above discussion on the vortex mode selection and is consistent with the results in Stansby (1976), Karniadakis and Triantafyllou (1989) and Lu and Sato (1996). As expected, Fig. 5 also indicates that the peak of C_L corresponds approximately to the natural frequency. The same behavior was also found for a transversely oscillating cylinder in a uniform flow by Lu and Dalton (1996). This behavior reflects that large perturbations are generated as the cylinder is rotationally oscillated at or near the natural frequency, and is in good agreement with the experimental result in Filler et al. (1991) that large velocity fluctuations are observed in the shear layer with a high response peak at the natural frequency.

4.2. Timing of Vortex Formation

Figures 6 and 7 show the instantaneous vorticity contours and streamlines, respectively, observed in a fixed frame at

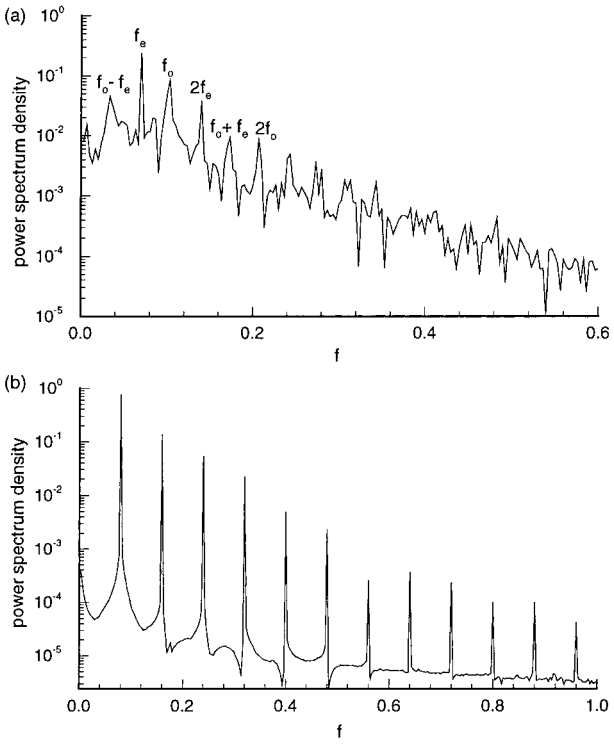

FIGURE 4 Power spectrum density of C_L for $\theta_{max} = 45°$, Re = 300, and f_e = (a) 0.07, (b) 0.08.

the cylinder for $f_e = 0.08$, $\theta_{max} = 45°$, and Re = 300 at four instants during a half period of the counterclockwise rotation. Note that the rotary oscillation frequency here is lower than the natural frequency, i.e. $f_o = 0.103$. When the counterclockwise rotation is started, as shown in Fig. 6a, a negative vortex is forming in the upper side behind the cylinder, and a positive one is located at the bottom of the cylinder. Then as the forcing rotational velocity is accelerated, the negative vortex is gradually grown up, and the positive one is convected to downstream (Fig. 6b). In Fig. 6c, the rotational velocity reaches the maximum value, the negative vortex located at the upper side of the cylinder becomes stronger. Meanwhile the positive vortex is shedding into the wake. When the rotational velocity is decelerated, another positive vortex is generated located at the lower side of the cylinder, and the negative vortex is continually grown up (Fig. 6d). Then, the rotation velocity is decelerated to zero at the instant of half period. At further time, when the clockwise rotation starts, the aforestated procedure is repeated in the opposite direction. During the following oscillation cycle, the vortex formation procedure is repeated. Accordingly, the streamlines pattern, as shown in Fig. 7, which corresponds to the vortex formation in Fig. 6, can clearly represent the near-wake topology behind the rotary cylinder. Apparently, a clockwise vortex is formed and

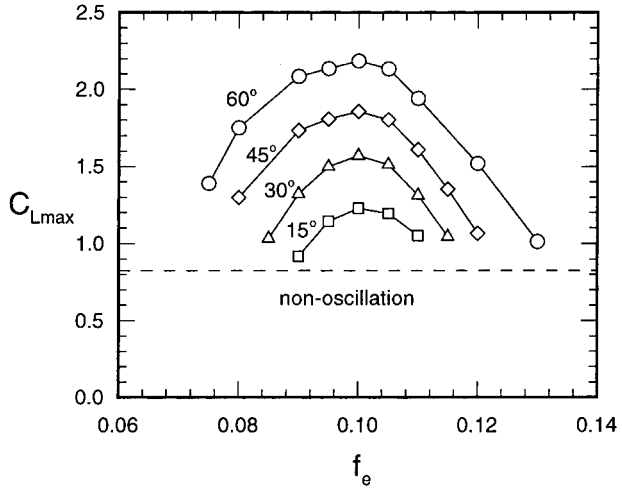

FIGURE 5 Distribution of the maximum values of C_L in the lock-on region for Re = 300.

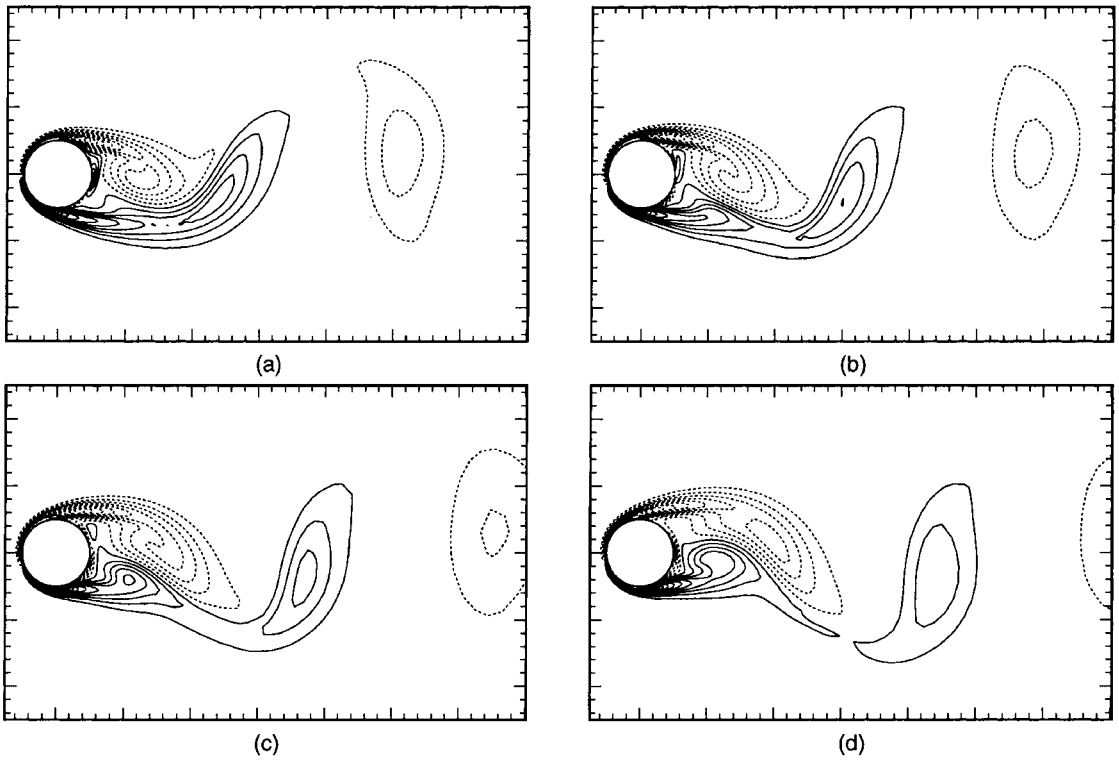

FIGURE 6 Vorticity contours for $\theta_{max} = 45°$, Re = 300, and $f_e = 0.08$ at t = (a) 0, (b) $0.125T_e$, (c) $0.25T_e$, (d) $0.375T_e$. Here, the solid lines represent positive values (counterclockwise vortex) and dashed lines negative values (clockwise vortex).

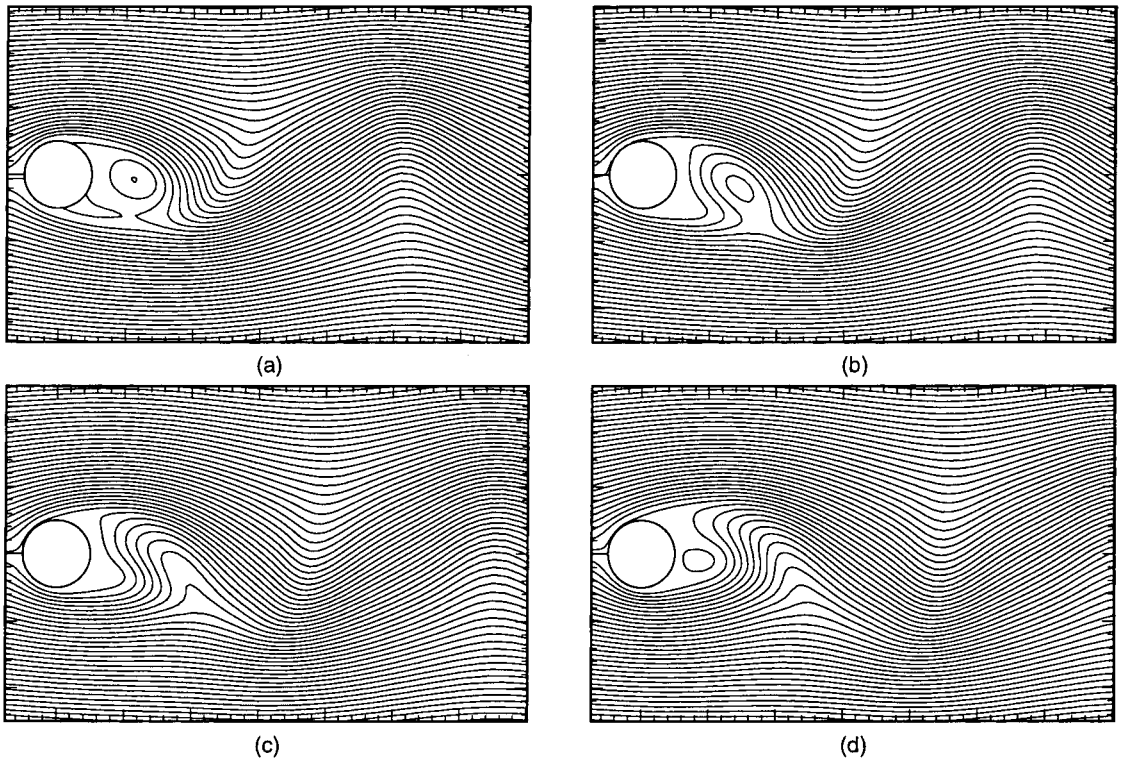

FIGURE 7 Streamlines for $\theta_{max} = 45°$, Re = 300, and $f_e = 0.08$ at t = (a) 0, (b) $0.125T_e$, (c) $0.25T_e$, (d) $0.375T_e$.

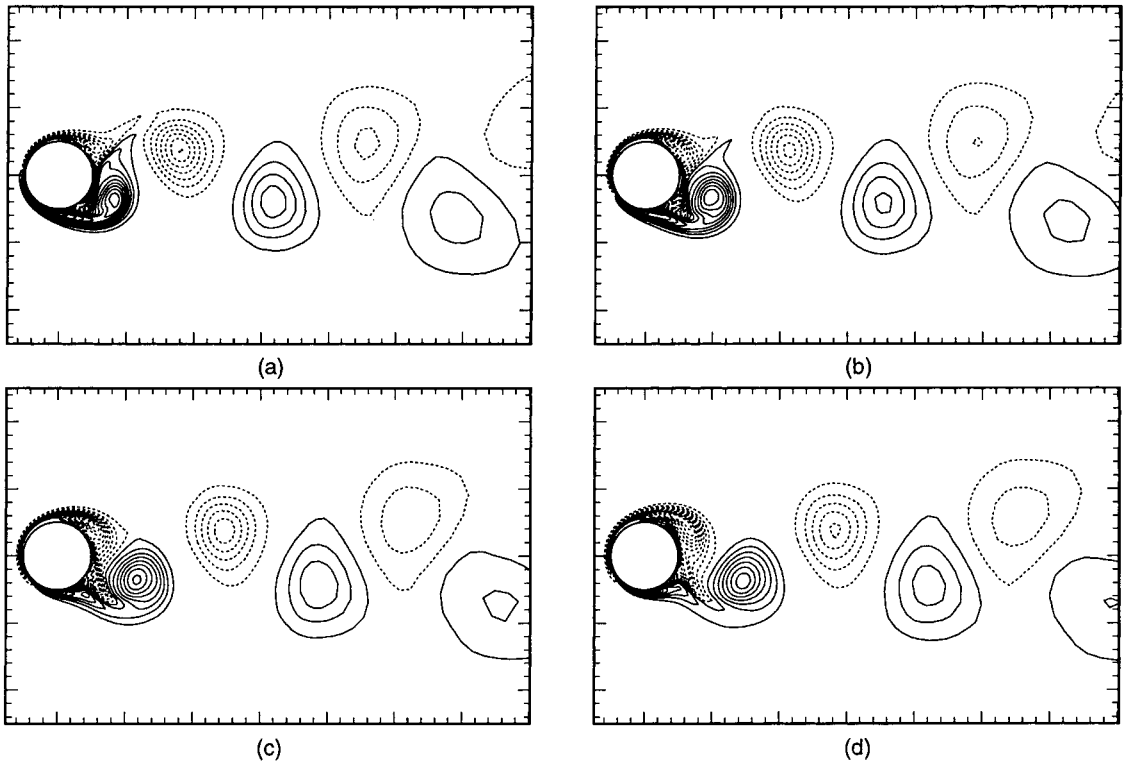

FIGURE 8 Vorticity contours for $\theta_{max} = 45°$, Re = 300, and $f_e = 0.12$ at t = (a) 0, (b) $0.125T_e$, (c) $0.25T_e$, (d) $0.375T_e$.

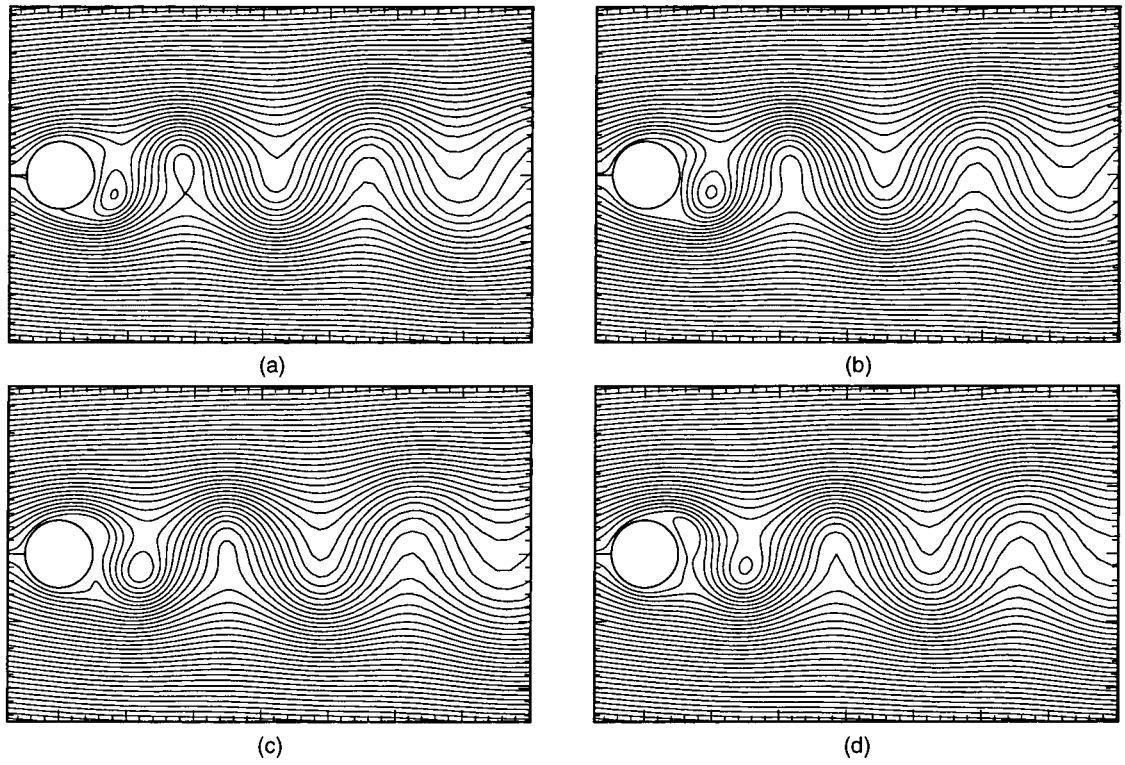

FIGURE 9 Streamlines for $\theta_{max} = 45°$, Re = 300, and $f_e = 0.12$ at t = (a) 0, (b) $0.125T_e$, (c) $0.25T_e$, (d) $0.375T_e$.

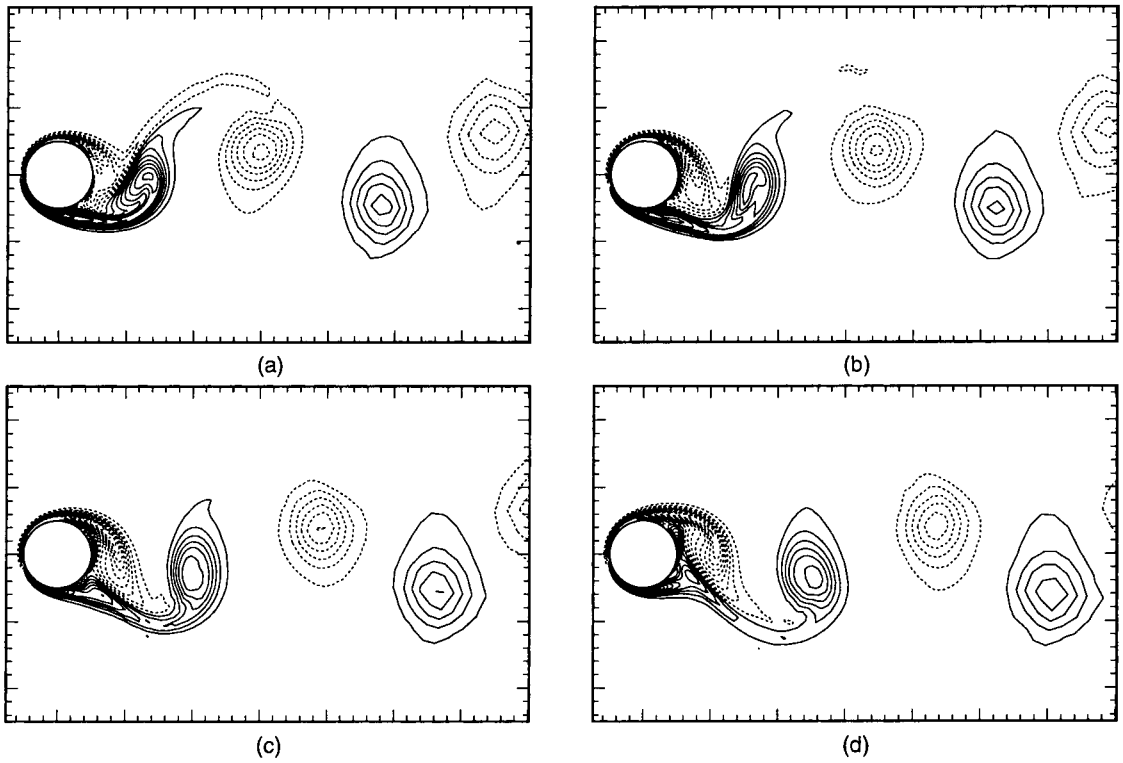

FIGURE 10 Vorticity contours for $\theta_{max} = 45°$, Re = 300, and $f_e = 0.1$ at t = (a) 0, (b) $0.125T_e$, (c) $0.25T_e$, (d) $0.375T_e$.

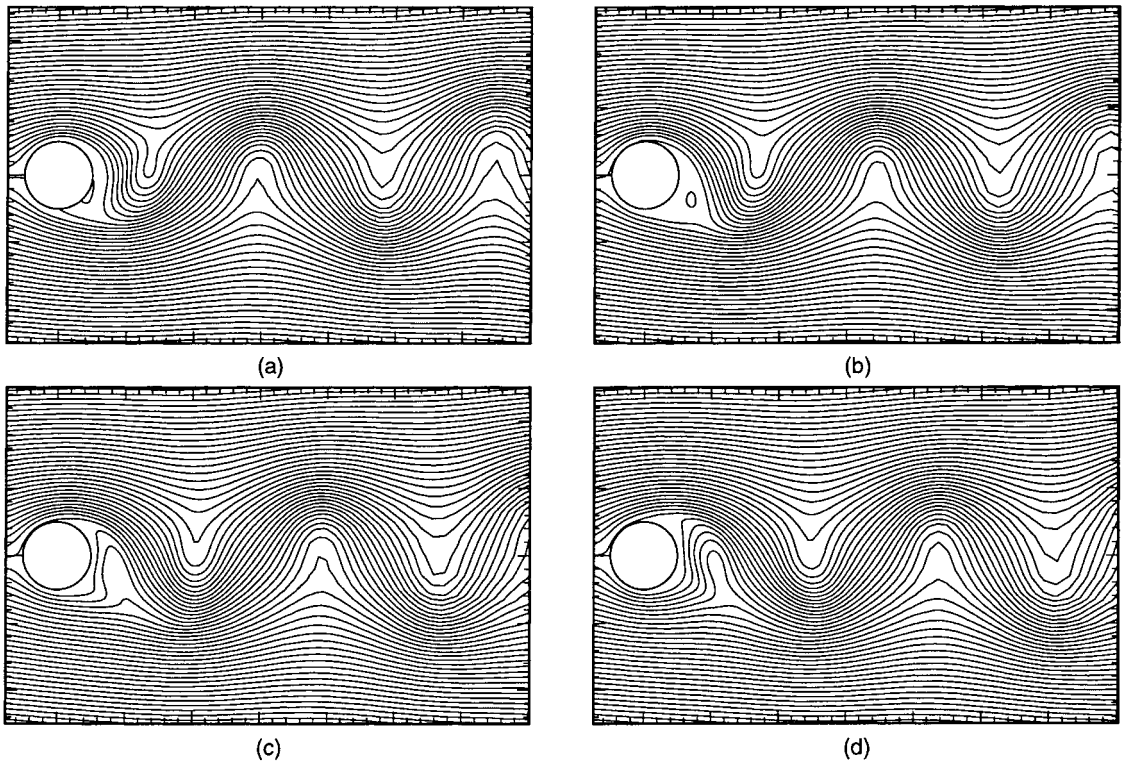

FIGURE 11 Streamlines for $\theta_{max} = 45°$, Re = 300, and $f_e = 0.1$ at t = (a) 0, (b) $0.125T_e$, (c) $0.25T_e$, (d) $0.375T_e$.

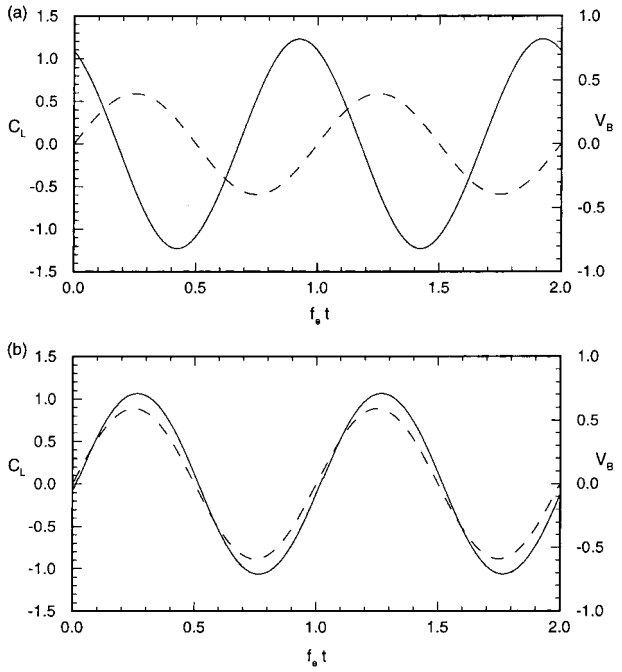

FIGURE 12 Lift coefficient (C_L) evolution with respect to rotary velocity (V_B): (a) $f_e = 0.08$, (b) $f_e = 0.12$. The solid line represents C_L and the dashed line V_B.

shed behind the cylinder in Figs. 7a and b. And a counterclockwise vortex begins to form as shown in Figs. 7c and d.

Figure 8 shows the vorticity contours for $f_e = 0.12$ and $\theta_{max} = 45°$, which is higher than the natural frequency. The instantaneous vorticity contours are displayed during the counterclockwise half period. As the cylinder starts to rotate in the counterclockwise direction, a positive vortex is generated located at the lower side of the cylinder, and a negative vortex is detached from the cylinder as shown in Fig. 8a. As the angular velocity increases, the positive vortex is grown up and the negative one is convected to downstream (Figs. 8b and c). Then, when the rotational velocity is decelerated, the positive vortex in the lower side of the cylinder becomes stronger to shed into downstream. Meanwhile, a negative vortex is gradually generated. At further time, after the rotation reverses, the vortex formation is repeated in the opposite direction. The corresponding streamlines are also shown in Fig. 9. It is also confirmed that a counterclockwise vortex is formed and shed behind the cylinder in Figs. 9a and b, and a clockwise vortex begins to form as shown in Figs. 9c and d. Comparing Fig. 9a with Fig. 7a, the initially formed concentration of vorticity abruptly switches to the opposite side of the cylinder as the forcing frequency is from $f_e = 0.08$ to 0.12, which is increased relative to the natural vortex formation frequency $f_o = 0.103$.

To illustrate the transient change of vortex formation by increasing the rotary oscillation frequency gradually, Figs. 10 and 11 show the instantaneous vorticity contours and streamlines, respectively, for $f_e = 0.1$ and $\theta_{max} = 45°$, which corresponds approximately to the natural frequency $f_o = 0.103$. Compared with the vortex formation shown in Figs. 6a and 8a, when f_e increases, the position of the positive vorticity in the lower side of the cylinder moves closer to the cylinder. Meanwhile, as shown in Figs. 6d, 8d and 10d, note the elongated vortex attached to the upper side of the cylinder; its length is decreasing when f_e increases. As expected, the longitudinal distance of the vortex street behind the cylinder increases with f_e decreasing.

Comparing Figs. 6 and 7 at $f_e = 0.08$ with Figs. 8 and 9 at $f_e = 0.12$, the switch in phase of the initially formed vortex can be identified. It is evident that whether the phase switch occurs or not mainly depends on the rotational frequency. To quantitatively characterize the phase of the vortex formation relative to the oscillating rotation velocity (V_B), the lift coefficient (C_L) distributions are shown in Fig. 12 for $f_e = 0.08$ and 0.12. From Fig. 12, the phase shift of C_L relative to V_B is approximately 241.8° at $f_e = 0.08$ and 2.6° at $f_e = 0.12$. So, when f_e is lower than the natural frequency, i.e. $f_o = 0.103$, C_L is out of phase with respect to V_B. To clarify the switch of vortex formation depending on the forcing condition, as shown in Fig. 6a, the initial counterwise vortex is formed on the upper side of the cylinder when the counterclockwise rotation is started; the cylinder is thus forced upwind and C_L is positive. During the acceleration phase, the C_L decreases to negative value. As f_e is higher than f_o, C_L is approximately in phase with V_B. Consequently, as shown in Fig. 8a, the initial counterclockwise vortex is generated from the lower side of the cylinder, when the cylinder starts to rotate in the counterclockwise direction. At this instant, C_L is nearly zero. Then in the acceleration phase, the C_L increases to positive value. To obtain a more complete picture of the phase of the vortex formation relative to the oscillatory forcing, Fig. 13

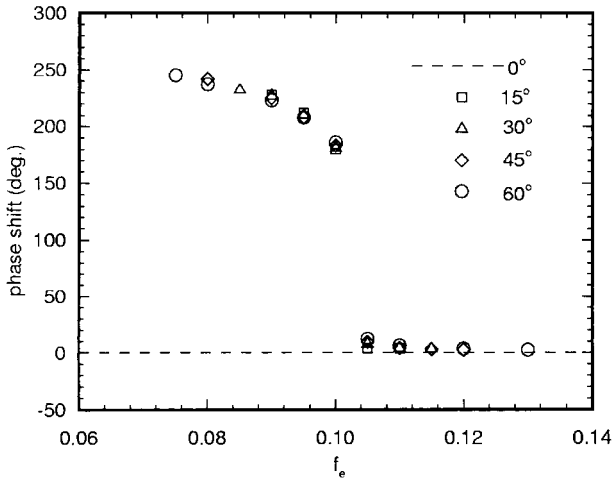

FIGURE 13 Phase shift of C_L relative to V_B for different f_e and θ_{max} at Re = 300.

shows the phase shift of C_L relative to V_B for different f_e and θ_{max} at Re = 300, corresponding to Fig. 5 for the distribution of the maximum values of C_L in the lock-on region.

To confirm the switch in phase of the vortex formation, several cases for different values of $\theta_{max}(\leq 90°)$ and Re($\leq$1000) were calculated further. It is verified that the switching phenomenon occurs in the neighborhood of the natural frequency. As f_e increases at a given θ_{max} and Re, the wake vorticity moves closer to the cylinder, eventually reaching a limiting position. This results in an abrupt switch of the vorticity concentration to the opposite side of the cylinder. The switch of initially formed vortex structure in the near wake of the cylinder was also found for forced transverse oscillation in a uniform flow experimentally by Ongoren and Rockwell (1988) and Gu et al. (1994), and numerically by Lu and Dalton (1996). Gu et al.(1994) found the switching phenomenon appeared at both low and high (185 and 5000) Reynolds numbers, even though the higher value of Re was larger enough for the Kelvin–Helmholtz instabilities to occur in the shear layers following separation. So, further studies are required to relate the switching phenomenon of the present problem to higher Re at which the Kelvin–Helmholtz instability occurs.

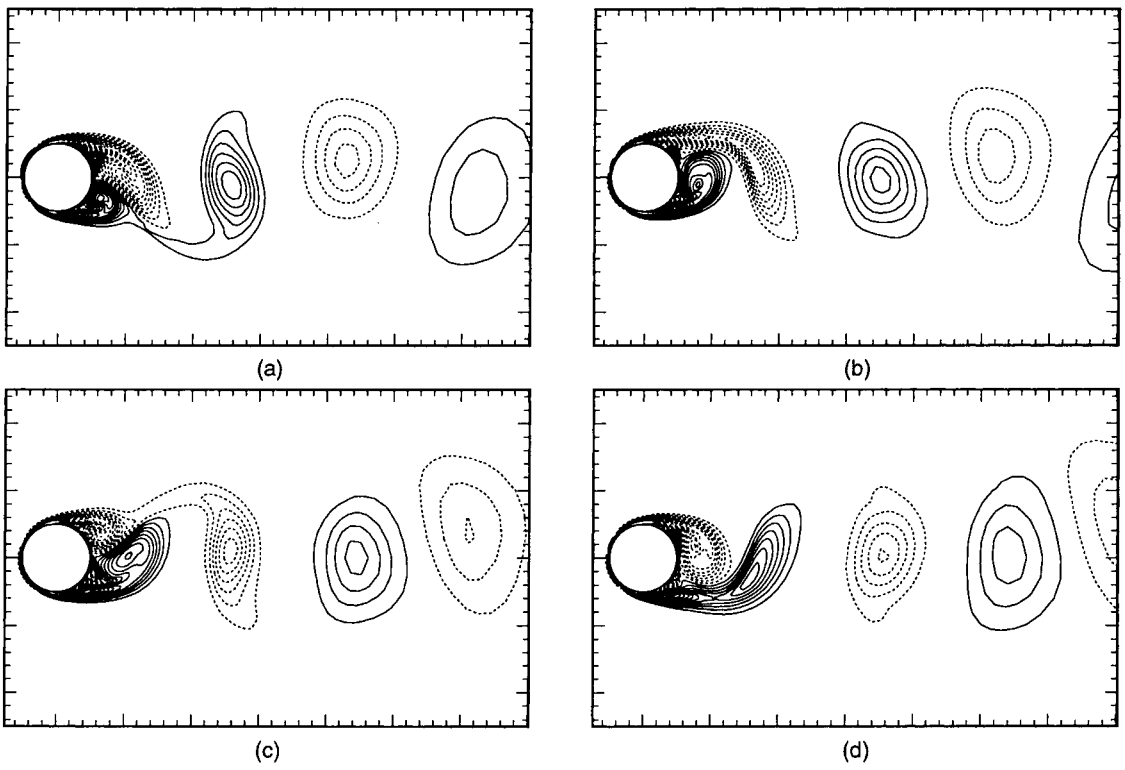

FIGURE 14 Vorticity contours for $\theta_{max} = 45°$, Re = 1000, and $f_e/f_o = 0.5$ at t = (a) $20T_e$, (b) $20.125T_e$, (c) $20.25T_e$, (d) $20.375T_e$.

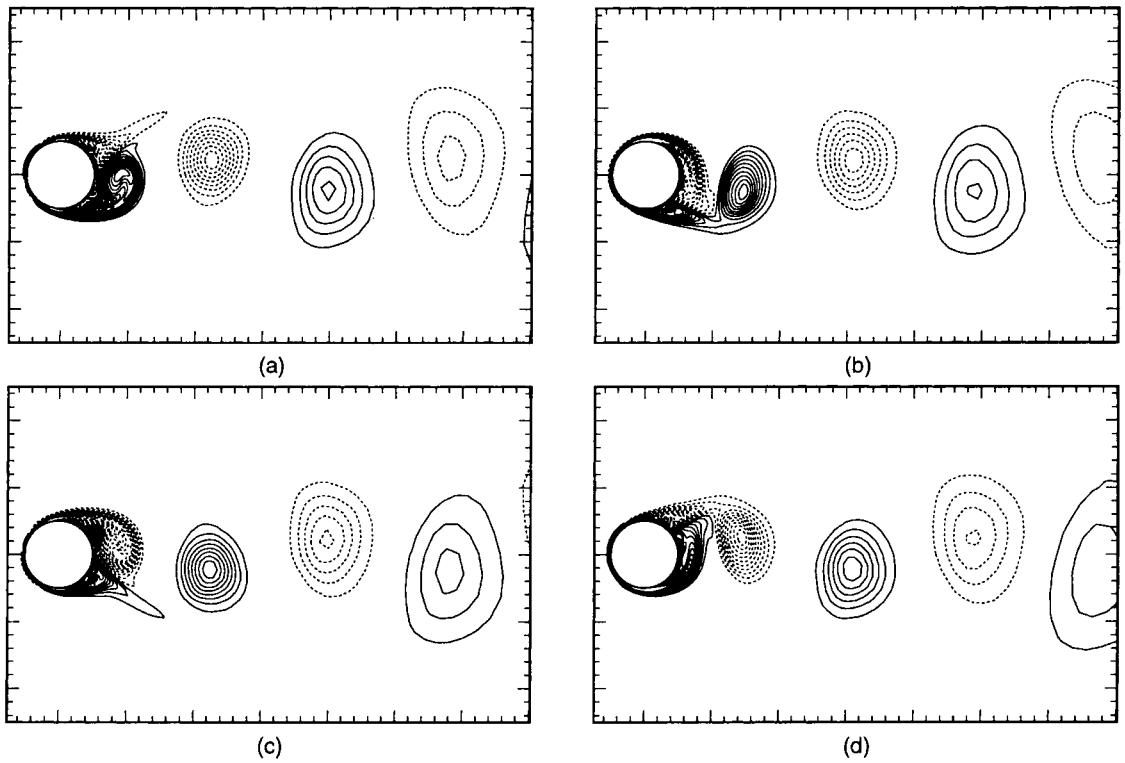

FIGURE 15 Vorticity contours for $\theta_{max} = 45°$, Re = 1000, and $f_e/f_o = 1$ at t = (a) $20T_e$, (b) $20.25T_e$, (c) $20.5T_e$, (d) $20.75T_e$.

4.3. Evolution of Vortex Formation

To demonstrate the vortex formation over a wider range of f_e, some typical cases, for a parameter range of $f_e/f_o = 0.5–4.0$, $\theta_{max} = 15–60°$, and Re = 1000, are discussed here. Based on calculated lift coefficient, the natural frequency is determined as $f_o = 0.11$ at Re = 1000. Several cases are exemplified for comparison, as

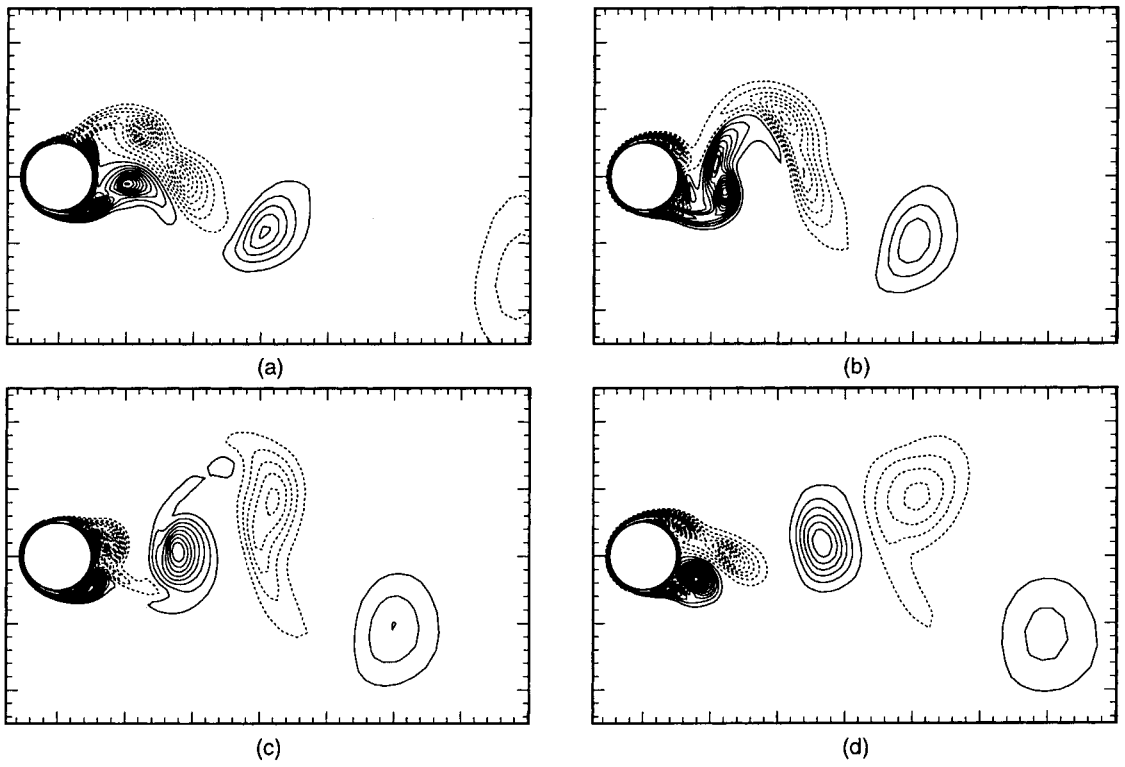

FIGURE 16 Vorticity contours for $\theta_{max} = 45°$, Re = 1000, and $f_e/f_o = 2$ at t = (a) $40T_e$, (b) $40.5T_e$, (c) $41T_e$, (d) $41.5T_e$.

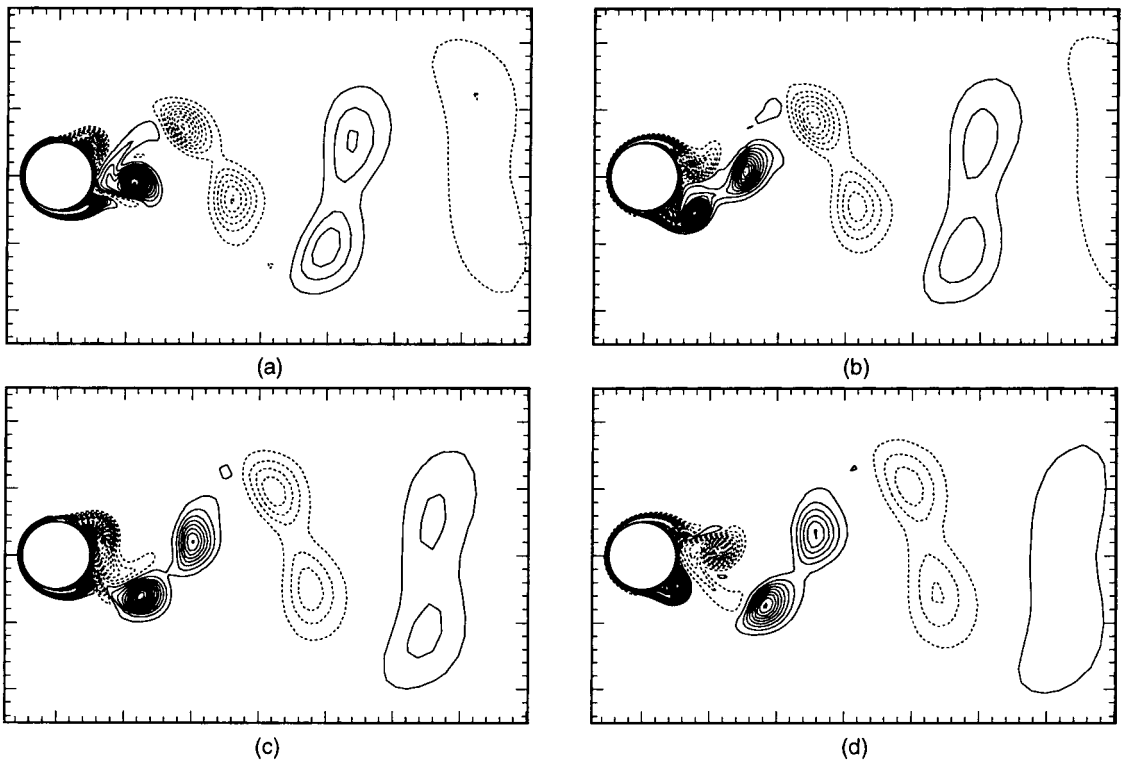

FIGURE 17 Vorticity contours for $\theta_{max} = 45°$, Re = 1000, and $f_e/f_o = 3$ at t = (a) $60T_e$, (b) $60.5T_e$, (c) $61T_e$, (d) $61.5T_e$.

shown in Figs. 14–18 for $\theta_{max} = 45°$, and $f_e/f_o = 0.5$, 1, 2, 3 and 4, respectively.

Figure 14 shows the instantaneous vorticity contours at four instants for $f_e/f_o = 0.5$. Note that these figures correspond to the results of only half oscillation period for $f_e/f_o = 0.5$. From Fig. 14, when the cylinder starts to rotate accelerately in the counterclockwise direction, one negative vortex is shed from the upper side of the cylinder

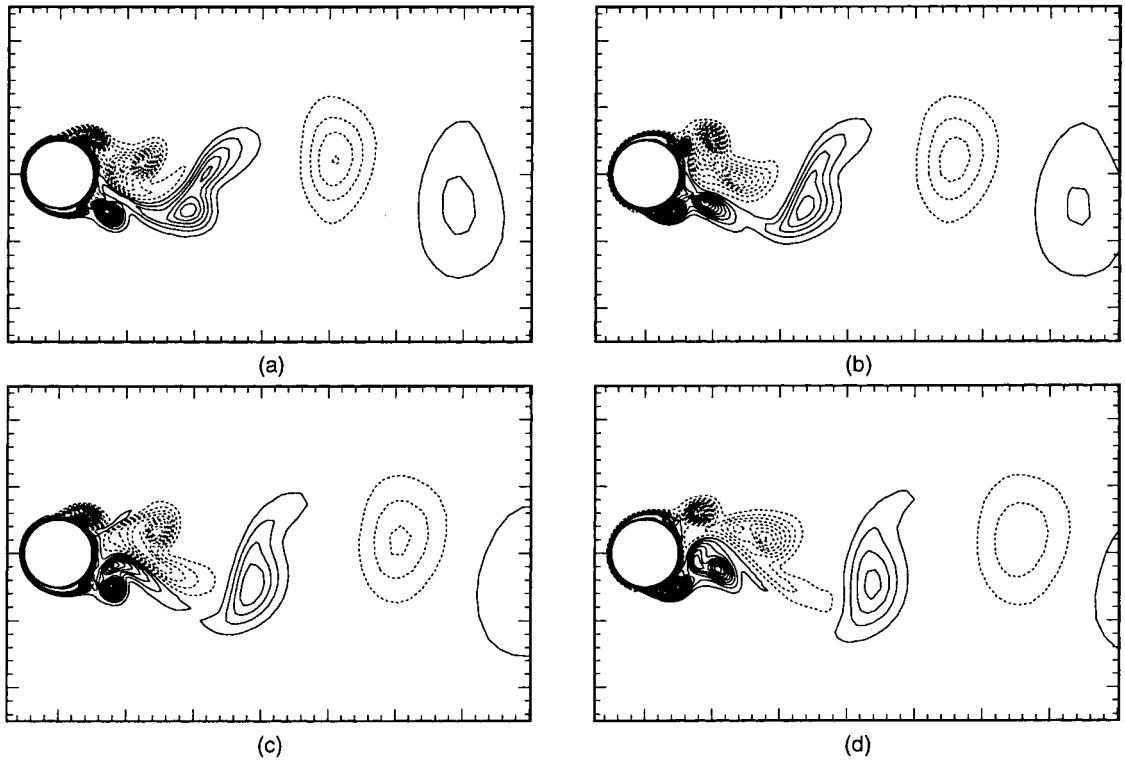

FIGURE 18 Vorticity contours for $\theta_{max} = 45°$, Re = 1000, and $f_e/f_o = 4$ at t = (a) $80T_e$, (b) $80.5T_e$, (c) $81T_e$, (d) $81.5T_e$.

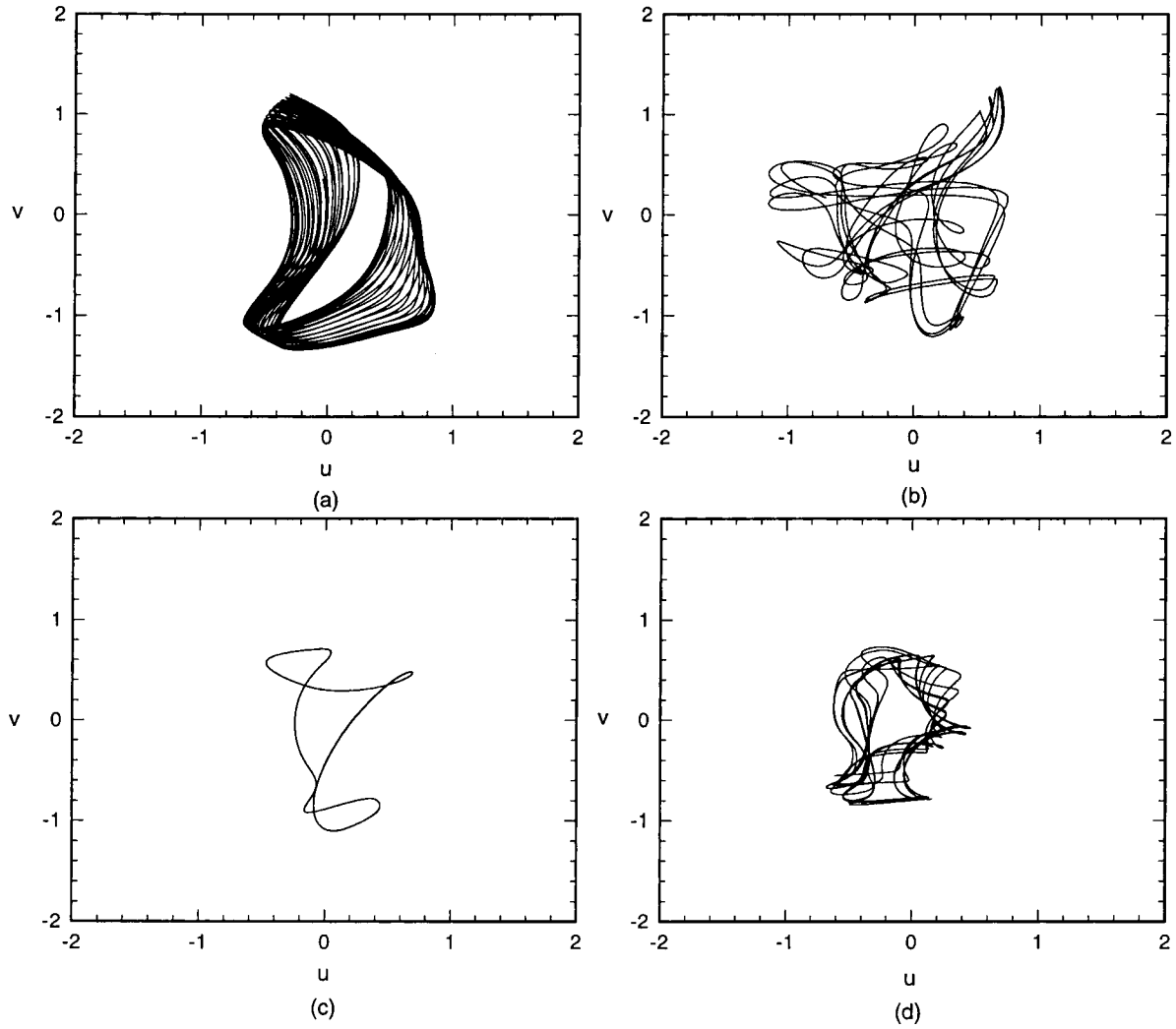

FIGURE 19 Phase diagram (velocity end-point diagram in u−vplane) at point of x = 1.8228 and y = 0.2704 for $\theta_{max} = 45°$, Re = 1000, and f_e/f_o = (a) 0.5, (b) 2, (c) 3 and (d) 4.

into the wake. As the cylinder is decelerated, one positive vortex is generated from the lower side of the cylinder and shed into the wake at further time. When the cylinder rotation reverses, the vortex formation is repeated in the opposite direction and both other negative and positive vortices are shed. The corresponding velocity phase diagram at one point in the near wake is displayed in Fig. 19a, which represents that the flow is quasi-periodic. Meanwhile, the lift and drag coefficients are shown in Fig. 20a. To determinate the vortex shedding frequency, the power spectrum density of the lift coefficient is calculated, as shown in Fig. 21a, where the highest peak corresponds to f_o which is consistent to the vortex shedding procedure as shown in Fig. 14. Other two cases were also calculated for the same oscillating frequency with $\theta_{max} = 30°$ and 60°. The vortex structures (not shown here) are similar to those given in Fig. 14.

Figure 15 shows the evolution of the vorticity contours for $f_e/f_o = 1$, which lays in the lock-on region. When the rotation starts in the counterclockwise direction, the initially vortex is generated in the lower side of the cylinder. During the first half period, the positive vortex is shed into wake. Meanwhile, a counter vortex is forming on the upper side of the cylinder. As the rotation reverses, the negative vortex is shed into downstream. In the following cycle, the vortex formation is repeated the above procedure. So, two opposite-sign vortices are shed from both the sides of the cylinder in one oscillating cycle. Some other cases were computed with different θ_{max} from 15 to 60° at $f_e/f_o = 1$; the similar vortex structures as shown in Fig. 15 were found. Further, several forcing frequencies, which lay in the lock-on regime and are lower and higher than f_o, were also calculated. The switching phenomena of the vortex formation were found at this Reynolds number.

As the forcing frequency increases, the instantaneous vorticity contours for $f_e/f_o = 2$ are shown in Fig. 16. Note that these figures correspond to the results of one and half oscillation periods. From Figs. 16a and b, two linked vortices with the same sign are shed from the upper side of the cylinder and one positive vortex is formed from the

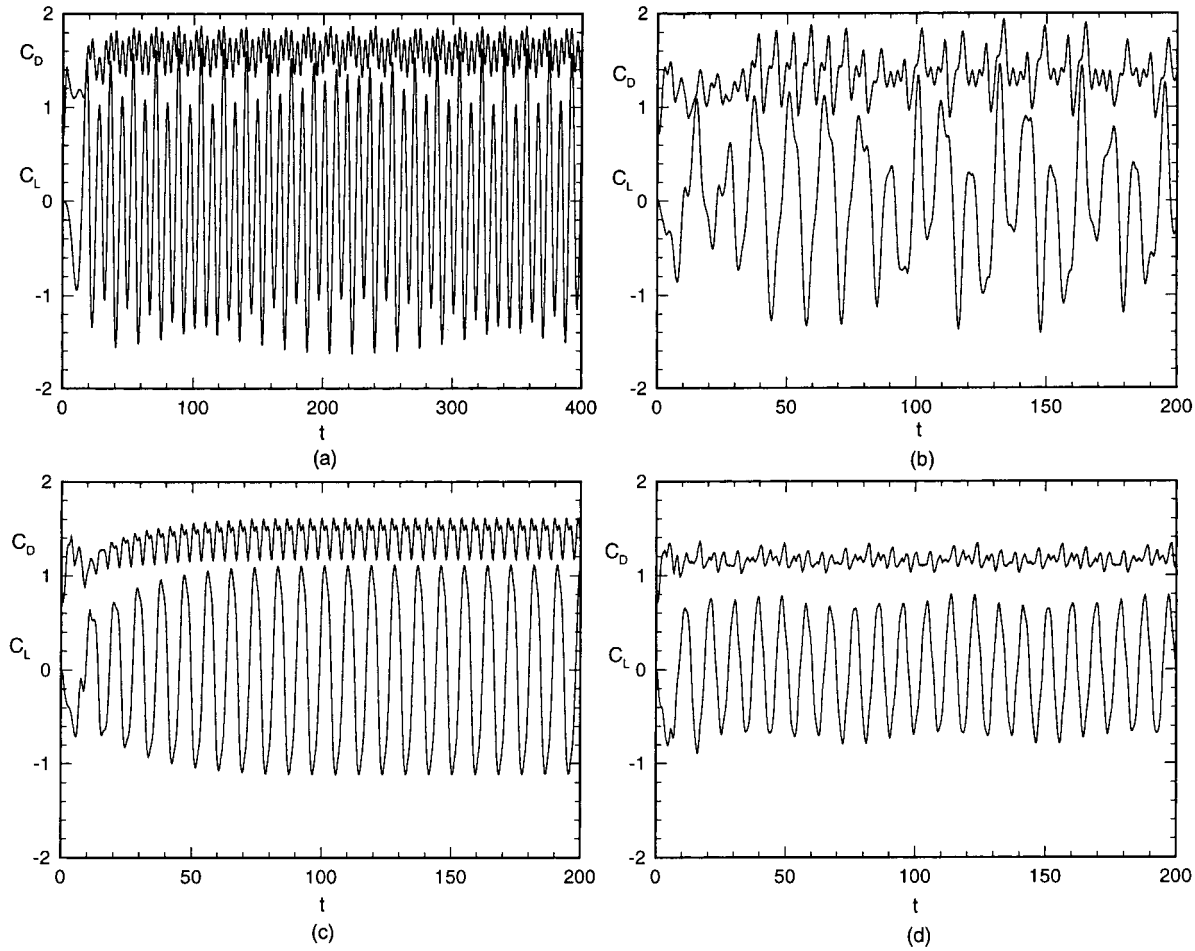

FIGURE 20 Lift and drag coefficients for $\theta_{max} = 45°$, Re = 1000, and $f_e/f_o =$ (a) 0.5, (b) 2, (c) 3 and (d) 4.

lower side of the cylinder. Then the linked vortices coalesce and are convected to downstream as shown in Fig. 16c. Meanwhile, the positive vortex is shed to wake. At further time, as shown in Fig. 16d, two negative vortices, which are linked together are generated and one positive is formed from both the sides of the cylinder. In this case, two same sign vortices and one opposite-sign vortex are shed from both the sides of the cylinder in one and half oscillating cycles. The similar vortex structures were also found experimentally by Williamson and Roshko (1988) and Ongoren and Rockwell (1988) for approach flows past a transversely oscillating cylinder.

Corresponding velocity phase diagram and the force coefficients are shown in Figs. 19b and 20b, respectively. Both Figs. 19b and 20b represent that the flow seems chaotic. From the power spectral analysis of C_L, as shown in Fig. 21b, the highest peak, denoted by f_s in Fig. 21b, is 0.0933, which is neither $f_e = 0.22$ nor $f_o = 0.11$. This behavior reflects the nonlinear effect on the flow evolution. Further studies are needed using nonlinear dynamic theory to analyze this behavior. Based on the present results, the similar flow features are found for $\theta_{max} = 15°$ and 60° with $f_e/f_o = 2$. However, as θ_{max} increases further, vortex shedding is synchronized with the cylinder oscillation, and the vortex shedding frequency is f_e. As an example, the instantaneous vorticity contours for $\theta_{max} = 90°$ are shown in Figs. 22a and b. There is an alternate, out-of-phase shedding of vortices from either side of the cylinder over an oscillating cycle. The wake takes on the appearance of two parallel vortex arrays, which coalesce together of the same sign vortices and decay in the near wake. The force coefficients are also given in Fig. 23a; the vortex shedding frequency calculated from Fig. 23a is equal to the forcing frequency. At this higher forcing frequency, the amplitude of C_L is smaller.

Figure 17 shows the evolution of the vorticity contours for $f_e/f_o = 3$. Note that these figures correspond to the results of one and half oscillation periods. From Fig. 17a, one positive vortex is formed from the lower side of the cylinder. In the following time, another positive vortex is generated again and linked with the previous one, as shown in Fig. 17b, then both the linked vortices are shed into the wake (Fig. 17c). From Fig. 17d, the linked vortices are convected into downstream and a counter vortex is formed from the upper side of the cylinder. At the next one and half oscillating cycles, the aforestated vortex formation procedure is repeated in the opposite direction. During each one and half cycles

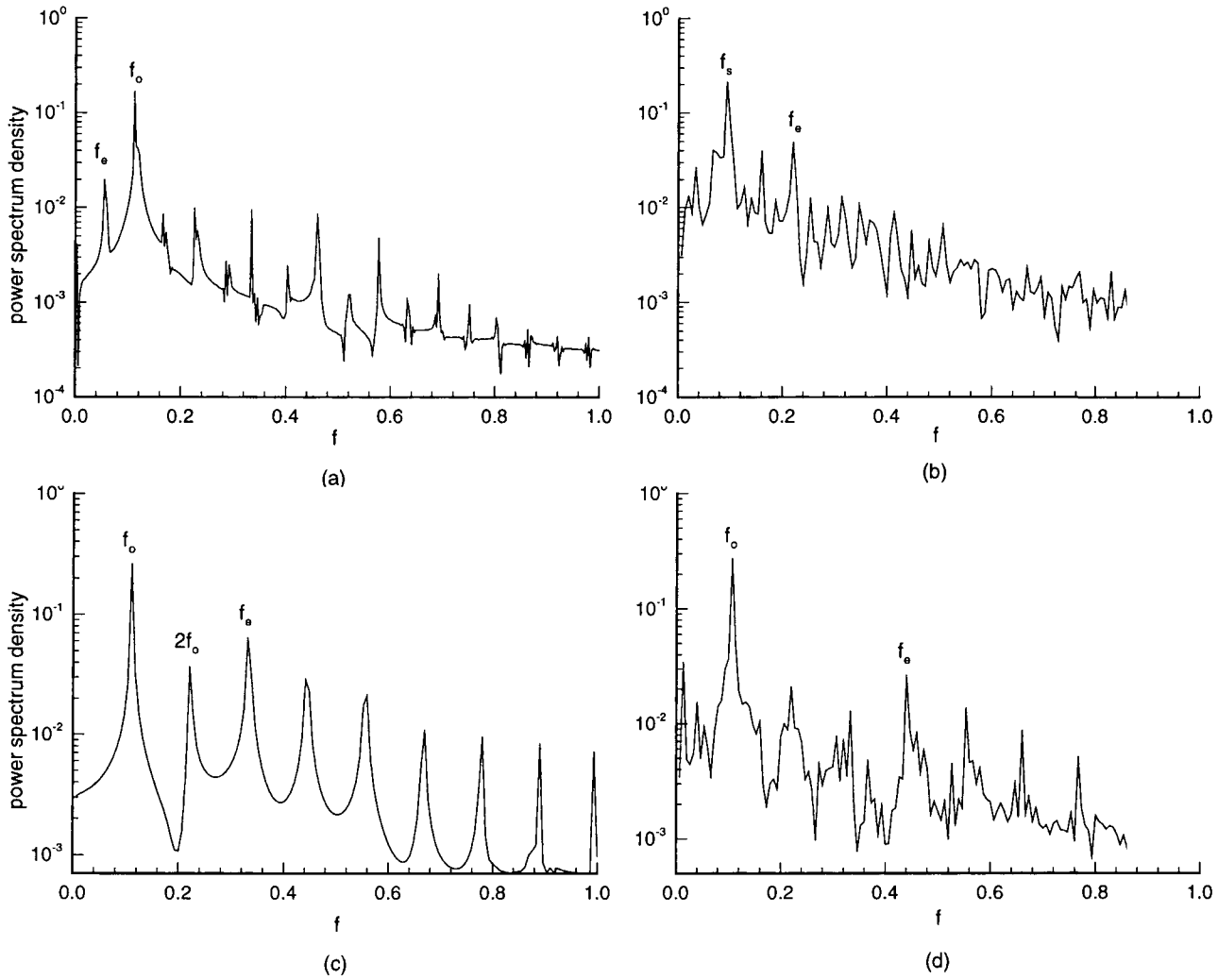

FIGURE 21 Power spectrum density of C_L for $\theta_{max} = 45°$, Re = 1000, and f_e/f_o = (a) 0.5, (b) 2, (c) 3 and (d) 4.

of the cylinder oscillation, the formation of two vortices with the same sign are shed from one side of the cylinder. Indeed, similar vortex structures, as shown in Fig. 17, are found experimentally for cross-flow oscillations of a cylinder by Williamson and Roshko (1988) and Sheridan et al. (1998), and for in-line oscillations of a cylinder by Griffin and Ramberg (1974) and Ongoren and Rockwell (1988). The corresponding velocity phase diagram and the force coefficients are shown in Figs. 19c and 20c, respectively, where periodic variation is identified.

At $f_e/f_o = 3$, very similar vortex structures, as shown in Fig. 17, were also found for $\theta_{max} = 30, 60°$ based on the present calculation. As θ_{max} increases further, a new vortex formation is formed. Figs. 22c and d show the instantaneous vorticity contours for $\theta_{max} = 90°$. The corresponding force coefficients are also given in Fig. 23b. The near-wake vortex structures lock to the cylinder oscillation, the vortex shedding frequency is f_e. Then the vortices of the same sign coalesce and disappear due to viscous dissipation. From Fig. 22, the vortex structures for both the oscillating frequencies, i.e. $f_e/f_o = 2$ and 3, are very similar. In general, the forcing frequency higher than a certain value takes a new mode in the shear layer characterized by smaller vortices of shorter wavelength and retards the onset of large scale vortex formation in the near wake.

Figure 18 shows the vorticity contours for $f_e/f_o = 4$ at four instants. Due to the higher forcing frequency, small-scale vortices are shed near the cylinder, and immediately coalesce into large-scale vortices at some distance downstream of the cylinder. Note that the longitudinal wavelength of the large-scale vortex street is approximately equal to that of the natural Karman vortex street. This is also confirmed by the variation of the force coefficients (Fig. 20d) and the power spectrum of C_L (Fig. 21d). It is identified that the highest peak in Fig. 22d corresponds to the natural frequency. From Fig. 19d for the velocity phase diagram, shorter wavelength oscillations, due to higher forcing frequency, are superimposed on the big velocity end-point drawn cycle which is related to the large-scale vortex formation in the downstream. Also, similar vortex structures were found for $\theta_{max} = 30$, 60° at this higher forcing frequency.

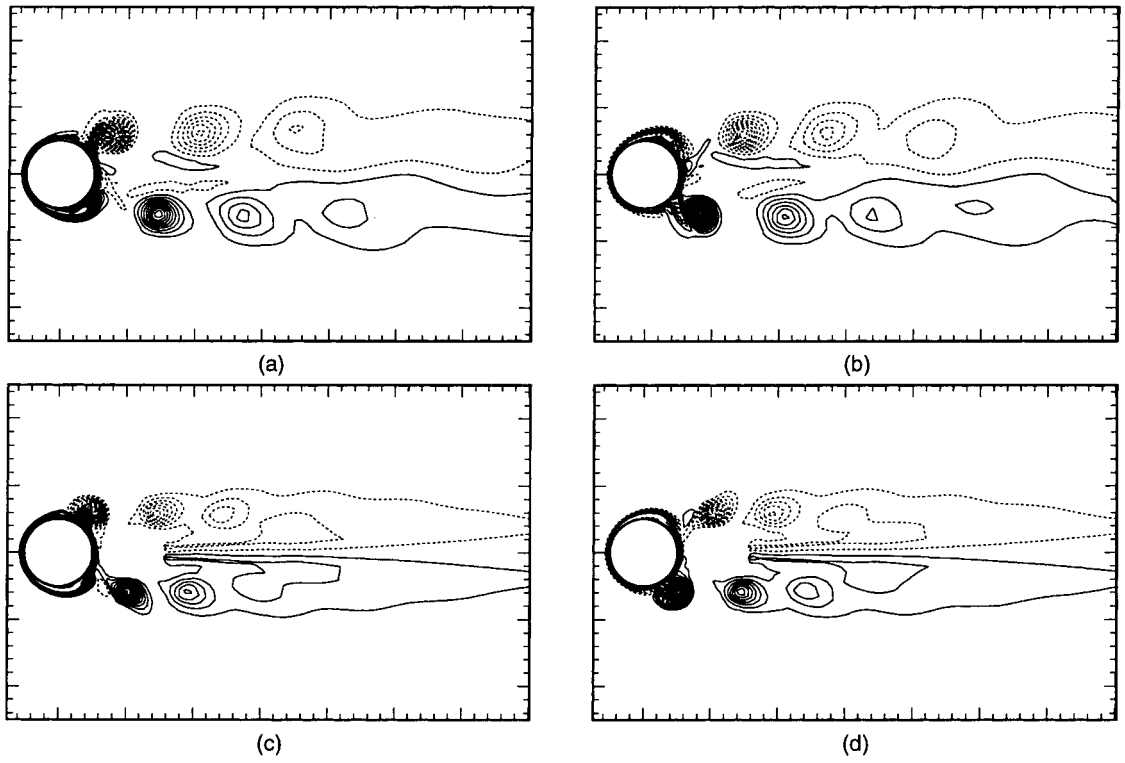

FIGURE 22 Vorticity contours for Re = 1000, and $\theta_{max} = 90°$: (a) t = 0, $f_e/f_o = 2$, (b) t = 0.5T_e, $f_e/f_o = 2$, (c) t = 0, $f_e/f_o = 3$, (d) t = 0.5T_e, $f_e/f_o = 3$.

5. CONCLUSIONS

The unsteady flow over a rotationally oscillating circular cylinder is numerically investigated by solving the two-dimensional incompressible Navier–Stokes equations. When the rotating oscillation frequency of the cylinder is in the vicinity of the natural vortex formation frequency, a lock-on vortex formation regime appears and becomes wider as the excitation amplitude is increased. As the excitation frequency is increased relative to the natural frequency, the initially formed concentration of vorticity moves closer to the cylinder until a limiting position is reached; at this point, the vorticity concentration abruptly switches to the opposite side of the cylinder. This process induces distinct changes of the phase between the external forcing and the forces acting on the cylinder. The effects of oscillating frequency and amplitude on the vortex structures are also studied, and some basic patterns of vortex shedding, based on the present calculated results, are identified.

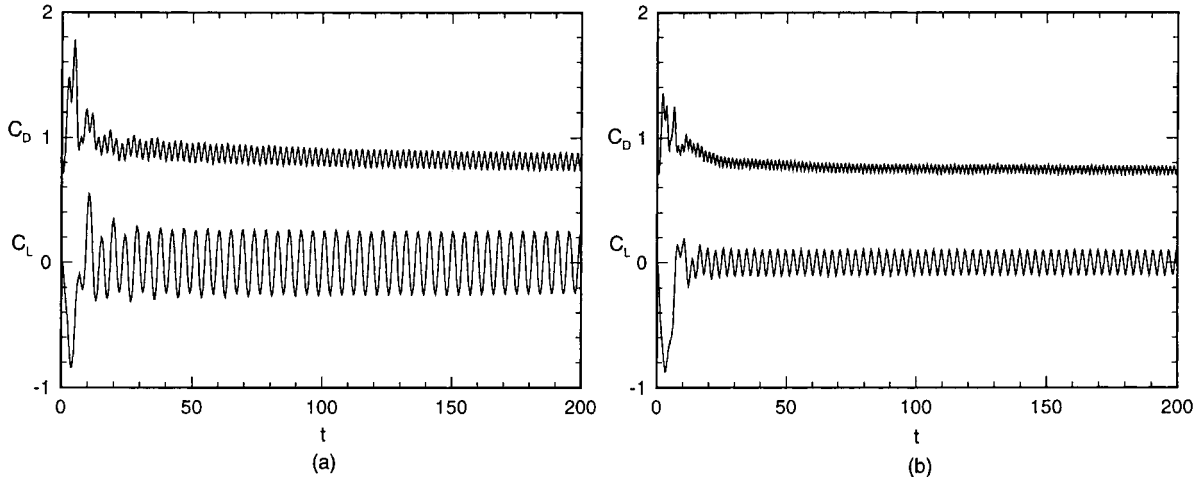

FIGURE 23 Lift and drag coefficients for Re = 1000, and $\theta_{max} = 90°$: (a) $f_e/f_o = 2$, (b) $f_e/f_o = 3$.

Acknowledgements

This work was supported by the Program of Chinese Academy of Sciences (CAS) Hundred Talents and the Program of the Trans-Century Outstanding Young Training of the Ministry of Education (MOE).

References

Badr, H.M. and Dennis, S.C.R. (1985) "Time-dependent viscous flow past an impulsively started rotating and translating circular cylinder", J. Fluid Mech. 158, 447–488.

Badr, H.M., Coutanceau, M., Dennis, S.C.R. and Ménard, C. (1990) "Unsteady flow past a rotating circular cylinder at Reynolds numbers 10^3 and 10^4", J. Fluid Mech. 220, 459–484.

Baek, S. and Sung, H.J. (1998) "Numerical simulation of the flow behind a rotary oscillating circular cylinder", Phys. Fluids 10, 869–876.

Baek, S.-J. and Sung, H.J. (2000) "Quasi-periodicity in the wake of a rotationally oscillating cylinder", J. Fluid Mech. 408, 275–300.

Barbi, C., Favier, D.P., Maresca, C.A. and Telionis, D.P. (1986) "Vortex shedding and lock-on of a circular cylinder in oscillatory flow", J. Fluid Mech. 170, 527–544.

Buldakov, E.V., Chernyshenko, S.I. and Ruban, A.I. (2000) "On the uniqueness of steady flow past a rotating cylinder with suction", J. Fluid Mech. 411, 213–232.

Chen, Y.M., Ou, Y.R. and Pearlstein, A.J. (1993) "Development of the wake behind a circular cylinder impulsively started into rotatory and rectilinear motion", J. Fluid Mech. 253, 449–484.

Dennis, S.C.R., Nguyen, P. and Kocabiyik, S. (2000) "The flow induced by a rotationally oscillating and translating circular cylinder", J. Fluid Mech. 407, 123–144.

Filler, J.R., Marston, P.L. and Mih, W.C. (1991) "Response of the shear layers separating from a circular cylinder to small-amplitude rotational oscillations", J. Fluid Mech. 231, 481–499.

Gresho, P.M. and Sani, R. (1987) "On pressure boundary conditions for the incompressible Navier–Stokes equations", Int. J. Numer. Methods Fluids 7, 1111–1145.

Griffin, O.M. and Ramberg, S.E. (1974) "The vortex streets of vibrating cylinders", J. Fluid Mech. 66, 553–576.

Gu, W., Chyu, C. and Rockwell, D. (1994) "Timing of vortex formation from an oscillating cylinder", Phys. Fluids 6, 3677–3682.

Karniadakis, G. and Triantafyllou, G. (1989) "Frequency selection and asymptotic states in laminar wakes", J. Fluid Mech. 199, 441–469.

Kawamura, T. and Kuwahara, K. (1984) "Computation of high Reynolds number flow around a circular cylinder with surface roughness", AIAA Paper, 84–0340.

Kim, J. and Moin, P. (1985) "Application of a fractional-step method to incompressible Navier–Stokes equations", J. Comput. Phys. 59, 308–323.

Kwon, K. and Choi, H. (1996) "Control of laminar vortex shedding behind a circular cylinder using splitter plates", Phys. Fluids 8, 479–486.

Lu, X.Y. (1996) "The early stage of development of the wake behind a circular cylinder impulsively started into rotatory and rectilinear motion", Trans. Japan Soc. Aero. Space Sci. 39, 11–27.

Lu, X.Y. and Dalton, C. (1996) "Calculation of the timing of vortex formation from an oscillating cylinder", J. Fluids Struct. 10, 527–541.

Lu, X.Y. and Sato, J. (1996) "A numerical study of flow past a rotationally oscillating circular cylinder", J. Fluids Struct. 10, 829–849.

Lu, X.Y., Dalton, C. and Zhang, J. (1997) "Application of large eddy simulation to an oscillating flow past a circular cylinder", ASME J. Fluids Engng. 119, 519–525.

Nakano, M. and Rockwell, D. (1993) "The wake from a cylinder subjected to amplitude-modulated excitation", J. Fluid Mech. 247, 79–110.

Ongoren, A. and Rockwell, D. (1988) "Flow structure from an oscillating cylinder. Part I, mechanisms of phase shift and recovery of the near-wake", J. Fluid Mech. 191, 192–223.

Park, D.S., Ladd, D.M. and Hendricks, E.W. (1994) "Feedback control of von Karman vortex shedding behind a circular cylinder at low Reynolds numbers", Phys. Fluids 6, 2390–2405.

Roussopoulos, K. (1993) "Feedback control of vortex shedding at low Reynolds numbers", J. Fluid Mech. 248, 267–296.

Sarpkaya, T. (1986) "Force on a circular cylinder in viscous oscillatory flow at low Keulegan–Carpenter numbers", J. Fluid Mech. 165, 61–71.

Sheridan, J., Carberry, J., Lin, J.-C. and Rockwell, D. (1998) "On the near-wake topology of an oscillating cylinder", J. Fluids Struct. 12, 215–220.

Stansby, P.K. (1976) "The locking-on of vortex shedding due to the cross-stream vibration of circular cylinders in uniform and shear flows", J. Fluid Mech. 74, 641–665.

Strykowski, P.J. and Sreenivasan, K.R. (1990) "On the formation and suppression of vortex shedding at low Reynolds numbers", J. Fluid Mech. 218, 71–107.

Taneda, S. (1978) "Visual observations of the flow past a circular cylinder performing a rotatory oscillation", J. Phys. Soc. Japan 45, 1038–1043.

Tokumaru, P.T. and Dimotakis, P.E. (1991) "Rotary oscillation control of a cylinder wake", J. Fluid Mech. 224, 77–90.

Tokumaru, P.T. and Dimotakis, P.E. (1993) "The lift of a cylinder executing rotary motions in a uniform flow", J. Fluid Mech. 255, 1–10.

Unal, M.F. and Rockwell, D. (1987) "On vortex formation from a cylinder: Part 2, control by splitter-plate interference", J. Fluid Mech. 190, 513–529.

Williamson, C.H.K. and Roshko, A. (1988) "Vortex formation in the wake of an oscillating cylinder", J. Fluids Struct. 2, 355–381.

Wu, J.Z., Lu, X.Y., Denney, A.G., Fan, M. and Wu, J.M. (1998) "Post-stall flow control on an airfoil by local unsteady forcing", J. Fluid Mech. 371, 21–58.